Article:
Kulmaczewski, R orcid.org/0000-0002-3855-4530, Bamiduro, F orcid.org/0000-0002-1914-5731, Shahid, N orcid.org/0000-0002-8090-7619 et al. (2 more authors) (2021) Structural Transformations and Spin-Crossover in [FeL2]2+ Salts (L = 4-{tertbutylsulfanyl}-2,6-di{pyrazol-1-yl}pyridine) − the Influence of Bulky Ligand Substituents. Chemistry: A European Journal, 27 (6). pp. 2082-2092. ISSN 0947-6539

https://doi.org/10.1002/chem.202004072

Structural Transformations and Spin-Crossover in $[Fe\mathit{L}_2]^{2+}$ Salts (L = 4-{*Tert*butylsulfanyl}-2,6-di{pyrazol-1-yl}pyridine) − the Influence of Bulky Ligand Substituents

Rafal Kulmaczewski,[a] Faith Bamiduro,[b] Namrah Shahid,[a] Oscar Cespedes[c] and Malcolm A. Halcrow*[a]

Abstract: 4-(*Tert*-butylsulfanyl)-2,6-di(pyrazol-1-yl)pyridine (*L*) was obtained in low yield from a one-pot reaction of 2,4,6-trifluoropyridine with 2-methylpropane-2-thiolate and sodium pyrazolate in a 1:1:2 ratio. The materials $[Fe\mathit{L}_2][BF_4]_2{\cdot}$solv (**1[BF$_4$]$_2$**·solv) and $[Fe\mathit{L}_2][ClO_4]_2{\cdot}$solv (**1[ClO$_4$]$_2$**·solv; solv = $MeNO_2$, MeCN or Me_2CO) exhibit a variety of structures and spin-state behaviors including thermal spin-crossover (SCO). Solvent loss on heating **1[BF$_4$]$_2$**·*x*$MeNO_2$ (*x* ≈ 2.3) occurs in two steps. The intermediate phase exhibits hysteretic SCO around 250 K, involving a "reverse-SCO" step in its warming cycle at a scan rate of 5 $Kmin^{-1}$. The reverse-SCO is not observed in a slower 1 $Kmin^{-1}$ measurement, however, confirming its kinetic nature. The final product $[Fe\mathit{L}_2][BF_4]_2{\cdot}0.75MeNO_2$ was crystallographically characterized, and shows abrupt but incomplete SCO at 172 K which correlates with disorder of an *L* ligand. The asymmetric unit of **1[BF$_4$]$_2$**·*y*Me_2CO (*y* ≈ 1.6) contains five unique complex molecules, four of which undergo gradual SCO in at least two discrete steps. Low-spin **1[ClO$_4$]$_2$**·$0.5Me_2CO$ is not isostructural with its BF_4^- congener, and undergoes single-crystal-to-single-crystal solvent loss with a tripling of the crystallographic unit cell volume, while retaining the $P\bar{1}$ space group. Three other solvate salts undergo gradual thermal SCO. Two of these are isomorphous at room temperature, but transform to different low-temperature phases when the materials are fully low-spin.

Introduction

Spin-crossover (SCO) compounds are molecular switches, where a transition ion undergoes a spin state change in response to a thermal, photochemical or pressure stimulus.[1-4] In condensed phases, this electronic rearrangement perturbs several other properties of a sample including its color, electrical resistance, dielectric constant and mechanical properties.[2,3,5] This gives SCO materials great promise as components in macro-, micro- and nano-scale devices.[4] More fundamentally, solid state SCO transitions are useful models for studies of crystal engineering,[6] and for fundamental mechanistic studies of crystallographic phase changes.[7] Iron(II) complexes of 2,6-di(pyrazol-1-yl)pyridine (bpp) derivatives are widely used in SCO research, since a wide range of substituents can be appended to the bpp framework.[8-10] Thus bpp derivatives bearing fluorescent,[11-13] photoactive,[14,15] redox-active,[16] conducting,[17] magnetic,[18,19] amphiphilic[20,21] and tether group substituents[13,22,23] have all been prepared, as have ditopic bpp ligands.[10,12,15,19,21,24,25] Iron complexes of these novel ligands often exhibit useful and/or multifunctional SCO switching properties. The unique availability of so many materials based on the same $[Fe(bpp)_2]^{2+}$ core also facilitates structure:function studies of SCO switching.[26,27]

Iron(II) complexes of bpp derivatives bearing 4-sulfanyl pyridyl substituents have consistently been SCO-active.[23,25,28,29] 4-(*Iso*propylsulfanyl)-2,6-di(pyrazol-1-yl)pyridine (bpp$^{S\mathit{i}Pr}$) proved particularly fruitful, in forming isostructural crystals of formula $[Fe(bpp^{S\mathit{i}Pr})_2]X_2{\cdot}$solv ($X^-$ = BF_4^- or ClO_4^-; solv = $MeNO_2$, Me_2CO, MeCN, EtCN, H_2O or sf [solvent-free]).[29,30] These solvates show unexpectedly different thermal and light-induced spin-state behaviors,[30] which can be correlated with reorientation and/or disordering of the lattice solvent between the spin states.[31]

In view of this, we were keen to investigate the bulkier analogue 4-(*tert*butylsulfanyl)-2,6-di(pyrazol-1-yl)pyridine (*L*) and its complexes $[Fe\mathit{L}_2]X_2$ (**1X$_2$**, Scheme 1). In contrast to the bpp$^{S\mathit{i}Pr}$ system, solvate crystals of **1X$_2$** exhibit a variety of structures and spin state properties, many of which are coupled to crystallographic symmetry breaking and other structural transformations. This includes a rare observation of "reverse" SCO during a slow desolvation process[32-35] and a rare example of a high *Z'* crystal[36] undergoing SCO, apparently without a crystallographic phase change.[37]

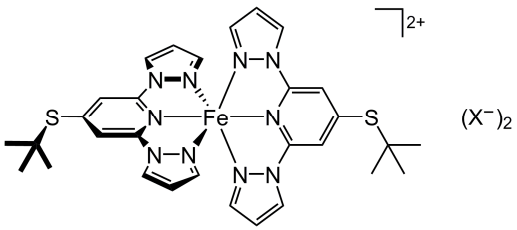

Scheme 1. Compound **1X$_2$** (X^- = BF_4^- or ClO_4^-).

[a] Dr. R. Kulmaczewski, N. Shahid, Prof. M. A. Halcrow
School of Chemistry, University of Leeds, Woodhouse Lane, Leeds LS2 9JT, UK
E-mail: m.a.halcrow@leeds.ac.uk
[b] Dr. F. Bamiduro
School of Chemical and Process Engineering, University of Leeds, Leeds LS2 9JT, UK
[c] Dr. O. Cespedes
School of Physics and Astronomy, University of Leeds, E. C. Stoner Building, Leeds LS2 9JT, UK

Supporting information for this article is given via a link at the end of the document. Experimental data can also be obtained from the University of Leeds library at http://doi.org/10.5518/910.

Results and Discussion

We have previously prepared 4-alkylsulfanyl-2,6-di(pyrazol-1-yl)pyridine derivatives in moderate yields, by alkylation of 4-hydrosulfanyl-2,6-di(pyrazol-1-yl)pyridine[23,25] with iodoalkane reagents.[28,29] However our attempts to synthesize *L* by this route were unsuccessful, presumably reflecting the low reactivity of the 2-iodo-2-methylpropane electrophile. Rather, a one pot treatment of 2,4,6-trifluoropyridine with sodium 2-methylpropane-2-thiolate, followed by 2 equiv of pyrazole and sodium hydride, in warm thf afforded a complex mixture of products from which *L* could be isolated in a low but reproducible yield.

Crystallographic determination of two polymorphs of *L* confirmed its identity. The α- and β- forms adopt the monoclinic $P2_1/c$ space group, with three and one independent molecules per asymmetric unit respectively (Figures S2-S5). The conformations of the four unique molecules in the two polymorphs are essentially identical, with *transoid*-coplanar heterocyclic rings and S*t*Bu groups oriented perpendicular to the *tris*-heterocyclic core. The three unique molecules in α-*L* form a triangular array by interdigitation of their *tert*butyl groups in the (001) plane, which has approximate non-crystallographic C_3 symmetry (Figure S3). These propagate *via* the *c* glide into tubular stacks along [001], which have helical character from the disposition of the protruding heterocyclic rings; there are two helices of opposite handedness in the unit cell. Adjacent helices interact through a $\pi...\pi$ interaction between two of the unique molecules in the lattice. The molecular packing in β-*L* is less striking, and involves no noteworthy intermolecular interactions.

Complexation of $Fe[BF_4]_2{\cdot}6H_2O$ and $Fe[ClO_4]_2{\cdot}6H_2O$ by 2 equiv *L* in nitromethane yielded $[FeL_2][BF_4]_2$ (**1[BF$_4$]$_2$**) and $[FeL_2][ClO_4]$ (**1[ClO$_4$]$_2$**) as orange or yellow powders, after the usual work-up. Recrystallization of both complex salts from nitromethane, acetonitrile or acetone using diethyl ether antisolvent gave different single crystalline solvates with different stoichiometries, which are mostly not isostructural and exhibit different spin state properties. These will be discussed in turn.

Most unusual is **1[BF$_4$]$_2$**·*x*$MeNO_2$, where $x \approx 2.3$ in the freshly prepared material. Its crystals (phase 1; monoclinic, $P2_1/c$, $Z = 8$) were analyzed at 120 and 250 K, and contain two unique molecules of the complex per asymmetric unit (Figure S11). Both cation sites are low-spin at 120 K, but the onset of thermal SCO in molecule A at 250 K is evident from its metric parameters (Table S7). That is consistent with the magnetic data, which indicate the material is *ca* 20 % high-spin at 250 K (Figure 1). The non-integer solvent stoichiometry arises from one of the four solvent sites in the model, whose contents were refined as a disordered distribution of either one or two nitromethane molecules. This solvent site, and other disordered solvent and anion residues, occupy small channels in the lattice running parallel to the unit cell *a* direction. Nearest neighbor residues in the lattice only interact through Van der Waals contacts.

Magnetic susceptibility measurements of **1[BF$_4$]$_2$**·*x*$MeNO_2$ confirm it is low-spin below 140 K, and shows an extremely gradual thermal SCO on warming with a midpoint temperature $T_{½} \approx 320$ K (Figure 1, top). $\chi_M T$ sharply increases from 2.5 to 3.5 $cm^3mol^{-1}K$ just above that temperature, consistent with the sample becoming fully high-spin at 350 K. This behavior is irreversible when the sample is recooled, indicating a change in spin state properties which is probably triggered by loss of lattice solvent at these elevated temperatures.[38]

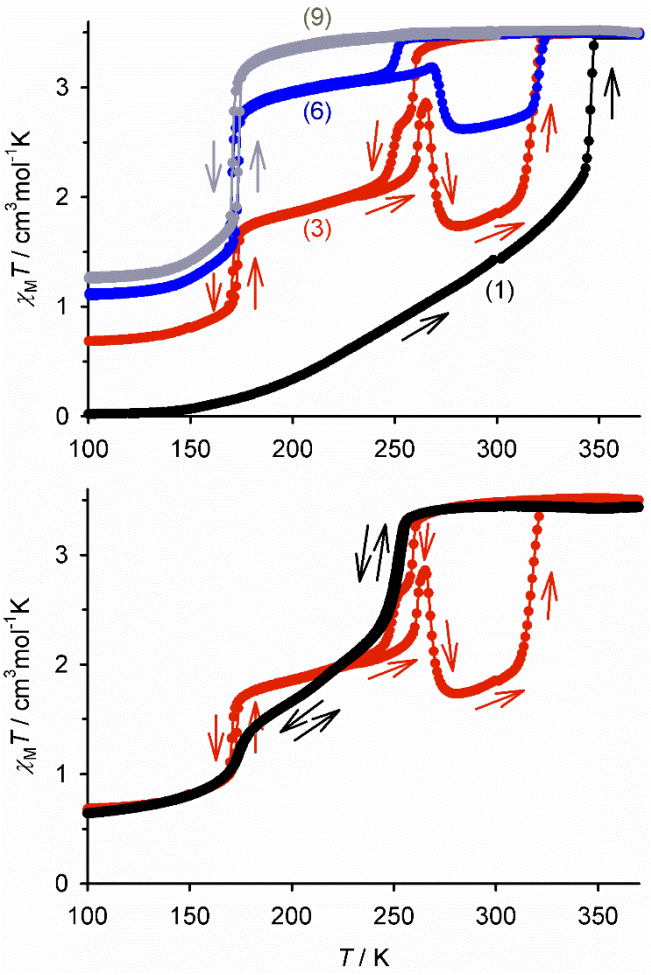

Figure 1 Top: Magnetic susceptibility data for **1[BF$_4$]$_2$**·*x*$MeNO_2$ upon multiple thermal scanning at 5 $Kmin^{-1}$. The first (black), third (red), sixth (blue) and ninth (gray) scans are shown. Bottom: overlaid magnetic data from annealed samples measured at 5 $Kmin^{-1}$ (scan 3, red) and 1 $Kmin^{-1}$ (black), Data points are linked by spline curves for clarity. Complete plots of all the scans in each experiment are in Figures S7-S9.

Repeated scanning of the sample between 5 and 370 K at 5 $Kmin^{-1}$ revealed two spin transition regimes, whose relative intensities change as the sample was aged (Figure 1, top; Figures S7 and S8). Scans 2 and 3 are dominated by an abrupt two-step spin-transition. One component occurs reversibly at $T_{½} = 260$ K, with no appreciable thermal hysteresis. The other step has $T_{½}\downarrow = 247$ K in cooling mode, and is associated with a "reverse" high→low-spin transition on rewarming, at $T_{½}\uparrow = 268$ K.[32-35] $\chi_M T$ retains a near-constant value after the reverse SCO event on further warming until 315 K, when the sample abruptly regains its fully high-spin state. While these transitions consistently decrease in intensity in later scans, the relative intensities of the two steps also evolve as the experiment proceeds. Most of the sample

undergoes the non-hysteretic classical spin transition in scan 2, but by scan 4 only the hysteretic reverse transition is visible in the data.

Another abrupt spin-transition near 170 K is also evident, which is very weak in scan 2 but develops in later scans at the expense of the higher temperature processes. By scan 9, only this transition is observed, where the sample undergoes an abrupt transition at $T_{½}$ = 172 K with a 3 K thermal hysteresis, to 50 % completeness. A more gradual SCO occurs on further cooling in the remainder of the sample until 140 K, where $\chi_M T$ reaches a value 1.3 $cm^3mol^{-1}K$ which remains constant until 30 K.[39] These data indicate *ca* 60 % of the sample undergoes SCO after completion of this experiment.

The measurement was repeated using a different annealed sample of **1[BF_4]$_2$**·*x*$MeNO_2$, at a slower scan rate of 1 $Kmin^{-1}$ (Figure 1, bottom). While the low temperature spin-transition is little changed by the slower scan rate, the processes near 250 K have collapsed into a more typical spin-transition, which occurs in two clear stages. An abrupt step at $T_{½}$ = 252 K, with a small hysteresis of 2 K, is followed by a more gradual decrease in $\chi_M T$ on further cooling centered near 210 K. The abrupt and gradual components of this transition involve approximately equal populations of iron centres ($\Delta\chi_M T$ = 1.0 $cm^3mol^{-1}K$ in both cases). The very different appearance of these transitions at the two scan rates confirms that the unusual features in the faster scans have a kinetic origin, which is discussed further below. In contrast to the first measurement, the composition of this sample was unchanged after six thermal cycles at 1 $Kmin^{-1}$ inside the SQUID magnetometer (Figure S9). The reason for that difference between the two experiments is unclear.[40]

These data indicate a sequence of phase changes in the sample, which slowly proceed as the sample is cycled during the 5 $Kmin^{-1}$ measurement. Two new phases are involved: the final product phase (phase 3) undergoing the partial SCO at 172 K; and, an intermediate phase 2 associated with the processes occurring near 250 K. TGA data were consistent with that view in showing two gradual but distinct mass losses summing to 5 % at 358 K, which corresponds to *ca* 0.8 equiv $MeNO_2$, and to 9.7 % at 423 K (1.5 equiv $MeNO_2$; Figure S6). Hence **1[BF_4]$_2$**·*x*$MeNO_2$ ($x \approx 2.3$) loses solvent in stepwise fashion on heating, and still retains *ca* 0.8 equiv of nitromethane at 423 K.

A single crystal of phase 3 was isolated from the SQUID magnetometer sample, after the repeated thermal cycling in Figure 1 (top) was complete. The crystal (orthorhombic, *Pbca,* Z = 8) had a reduced solvent content of $x \approx 0.75$, which agrees with the formulation after the second mass loss step in the TGA data. While the unit cell dimensions of phase 3 are similar to phase 1, phase 3 only contains one unique molecule per asymmetric unit. One *L* ligand in that cation is disordered over two equally occupied sites (Figure 2), which correspond to the ligand conformations in the two unique molecules of phase 1. Intermolecular steric clashes between the 'A' disorder sites of cations related by $-{}^1/_2+x$, y, ${}^1/_2-z$ and between the 'B' orientations of molecules related by ${}^1/_2+x$, y, ${}^1/_2-z$, imply each of these symmetry-related pairs of molecules must exist as an 'A/B' combination.

Full structure refinements from this crystal were achieved at 220 and 120 K, either side of its partial spin transition. While the metric parameters of the compound show it is fully high-spin at 220 K, at 120 K ligand disorder sites A and B are essentially high-spin and low-spin respectively (Table 1). That is consistent with the magnetic data from phase 3, which imply the compound is *ca* 60 % low-spin at that temperature (Figure 1, top). High-spin cations related to $[FeL_2]^{2+}$ whose structures deviate significantly from idealized D_{2d} symmetry often remain high-spin on cooling.[6,8] However, the geometry of the A and B cation sites is essentially the same within the error of the measurement (Table 1). Rather, we attribute the inability of site A to undergo SCO to a BF_4^- ion sandwiched between the site A *tert*butyl group and the heterocyclic core of the molecule (Figure 2). That should sterically inhibit displacement of that *tert*butyl group towards the iron atom, which would accompany the contraction of the Fe–N bonds associated with SCO.[41] There is no residue positioned to restrict movement of the *tert*butyl group in the SCO-active B disorder site (Figure S13).

The assignment of this crystal as phase 3 was confirmed by powder diffraction (Figure 3) and by variable temperature unit cell measurements, which show a clear discontinuity between 150-180 K (Figure S14). That corresponds to the temperature of the partial spin-transition in the final phase of the annealed sample (Figure 1, scan 9).

Table 1. Selected bond distances and angular parameters for phase 3 of **1[BF_4]$_2$**·*x*$MeNO_2$ [Å, °, Å^3]. See Figure 2 for the atom numbering scheme. Values separated by slashes correspond to the A and B disorder sites of the complex, respectively.[a]

T / K	220(2)	120(2)
Fe(1)–N(2)	2.140(4)	1.982(4)
Fe(1)–N(9)	2.196(5)	2.044(4)
Fe(1)–N(14)	2.175(5)	2.027(5)
Fe(1)–N(23)	2.134(14)/2.102(15)	2.123(14)/1.818(13)
Fe(1)–N(30)	2.140(5)	2.246(13)/1.889(8)
Fe(1)–N(35)	2.184(5)	2.046(12)/2.049(10)
V_{Oh}	12.02(3)/12.04(3)	10.95(3)/9.73(3)
Σ	155.6(10)/155.9(10)	138.6(13)/99.5(12)
Θ	497/495	451/290
ϕ	165.4(4)/165.5(4)	169.9(4)/171.4(4)
θ	76.75(5)/78.94(5)	81.41(8)/81.49(6)

[a] V_{Oh}, Σ and Θ are indices showing the spin state of the complex,[42,43] while ϕ and θ measure the relative orientations of the two tridentate ligands in the molecule.[44,45] Typical values for these parameters in $[Fe(bpp)_2]^{2+}$ derivatives are given in refs. [6] and [8].

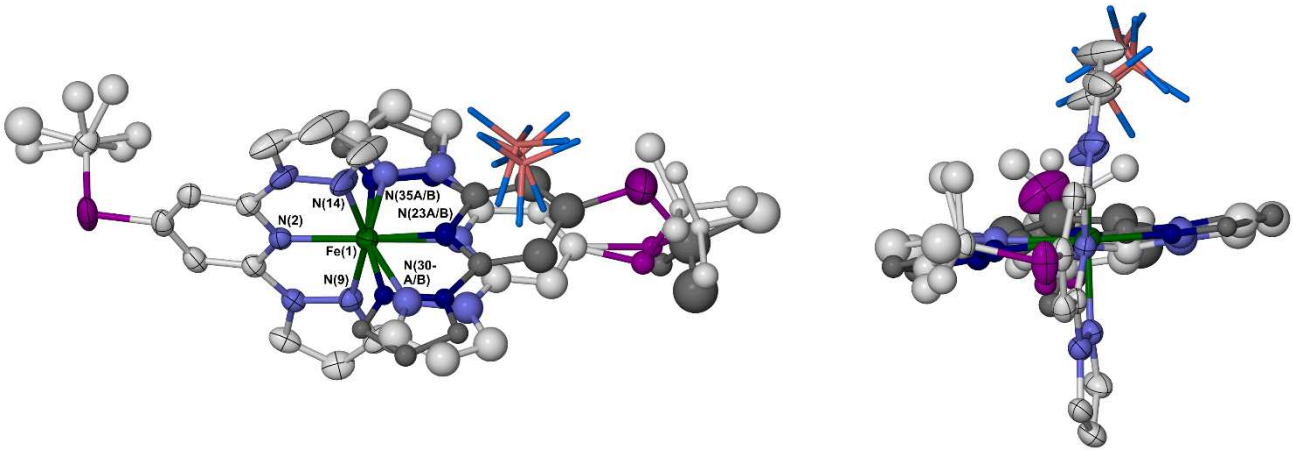

Figure 2 The complex cation in phase 3 of **1[BF_4]$_2$**·*x*$MeNO_2$, and the BF_4^- ion that could inhibit SCO in the 'A' ligand disorder orientation. All disordered residues in the molecule are shown, but H atoms are omitted for clarity. Displacement ellipsoids are at the 50 % probability level, except the disordered BF_4^- ion which is de-emphasized for clarity. The high-spin A and low-spin B ligand disorder orientations are highlighted with pale and dark coloration respectively. Color code: C, white or dark gray; B, pink; F, cyan; Fe, green; N, pale or dark blue; S, purple.

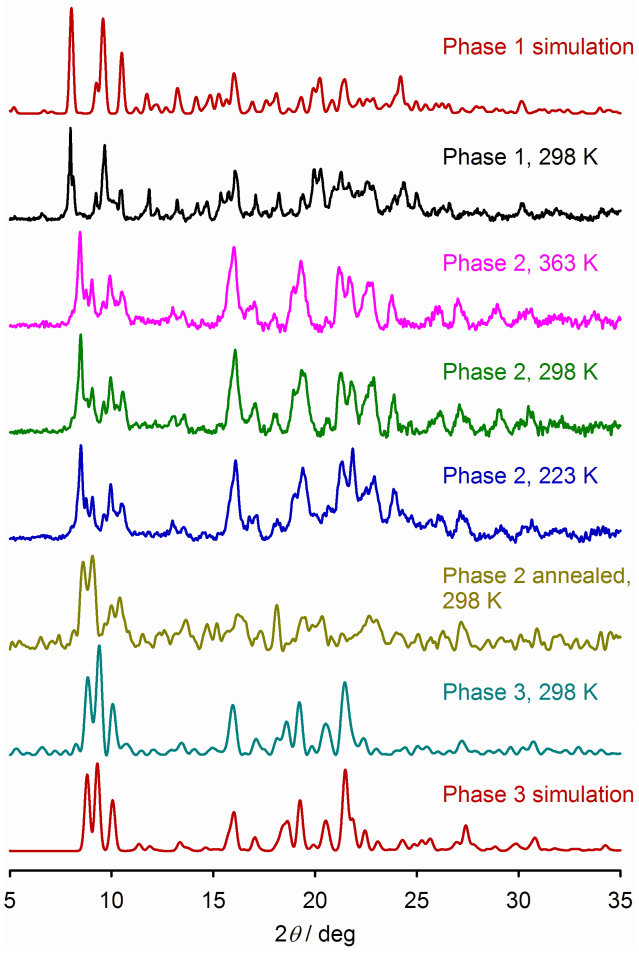

Figure 3 X-ray powder diffraction data for the different phases of **1[BF_4]$_2$**·*x*$MeNO_2$. The initial phase 1 powder pattern mostly matches the simulation, but with a few extra features suggesting minor desolvation may have occurred during the measurement. The annealed phase 2 sample was heated to 370 K for 1 hr, and is a mixture of phases 2 and 3.

Partial desolvation of phase 1 to phase 3 leads to substantial reorganization of its crystal packing, despite their similar unit cell dimensions (Figure 4). The channels of disordered anions and solvent in phase 1 are no longer present in phase 3, and the dispositions of the cations in the two lattices bear little relationship to each other. In phase 1, the cations pack loosely into layers along (001), and the two unique cation environments in the lattice are significantly canted with respect to each other (Figure 4, top). In phase 3 the cations form denser layers in the (010) plane, and are approximately co-aligned along the [001] vector (Figure 4, bottom). Notably, we only obtained a crystal of phase 3 on one occasion, and our attempts to convert phase 1 into phase 2 or 3 by annealing *in situ* led to crystal decomposition. Hence, it is unclear whether the phase 1→2→3 transformations occur in single-crystal-to-single-crystal fashion, or if our isolation of a phase 3 crystal from the multiply cycled SQUID sample was simply fortuitous.

Heating **1[BF_4]$_2$**·*x*$MeNO_2$ phase 1 to 370 K on a powder diffractometer causes its clean conversion to the intermediate phase 2 (Figure 3). The phase 2 powder pattern is retained with minor changes upon cooling from 360 to 223 K, showing the scan rate-dependent SCO in phase 2 is not associated with a crystallographic phase change. Heating phase 2 *in situ* at 370 K for 1 hr resulted in its incomplete conversion to phase 3. Further annealing the same sample at 370 K for 48 hrs did completely transform it to phase 3, however. The powder patterns of phase 1 and phase 3 agree well with their crystallographic simulations (Figure 3).

The reverse spin-transition shown by phase 2 in the 5 $Kmin^{-1}$ scans is rare, being thermodynamically disfavored on entropy grounds.[46] Such behavior can occur when a material undergoes different spin transitions at fast and slow scan rates, reflecting the involvement of a separate structural rearrangement with a similar timescale to the SQUID measurement. At intermediate scan rates the material relaxes its structure as the measurement proceeds, leading to a mid-transition switch from the "fast" to the "slow"

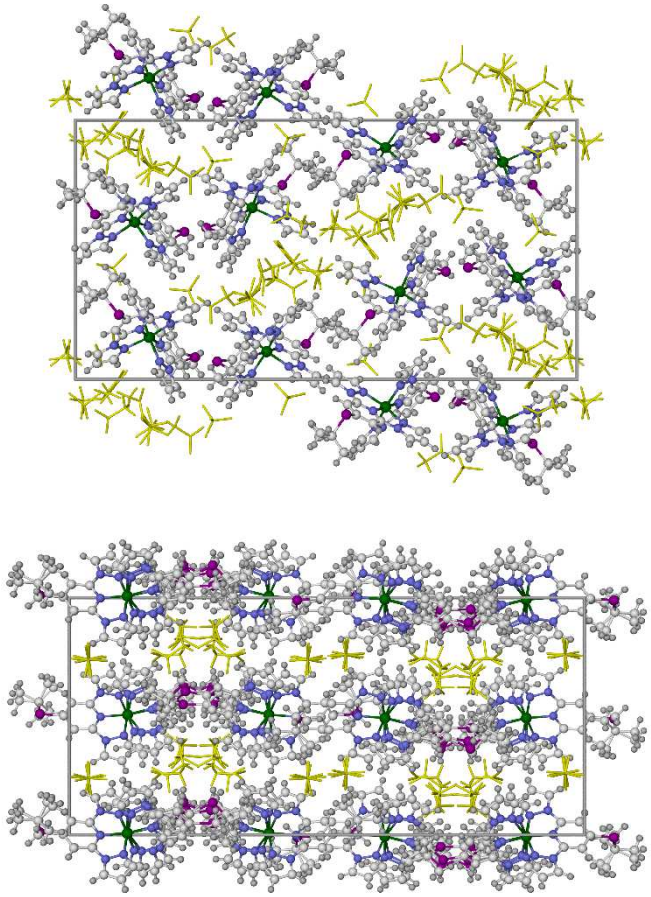

Figure 4 Packing diagrams of phase 1 (top) and phase 3 (bottom) of **1[BF_4]$_2$**·x$MeNO_2$ at 120 K. Both views are down the [100] crystal vector with the *c* axis horizontal. All disorder in the complex, anions and solvent is included in the Figure, and anions and solvent are de-emphasized for clarity. Color code: C{complex}, white; H{complex}, pale gray; Fe, green; N{complex}, blue; S, purple; BF_4^- and $MeNO_2$, yellow.

process in the warming branch of the $\chi_M T$ *vs* *T* curve. Examples are known where the fast and slow SCO regimes are related by reversible cleavage of a metal–ligand bond;[32] the conformational rearrangement of a ligand substituent;[33] or, redistribution of anions and solvent molecules within a lattice cavity.[34] The slow structure change during SCO most likely involves the *tert*butyl group conformations, or the anions or solvent in the lattice. Support for the former suggestion comes from the conformational flexibility of the S*t*Bu groups in the other solvates described below.

However, this interpretation implies the slow transition in the rapid scans exhibits *ca* 65 K thermal hysteresis (Figure 1, top). That hysteresis should be observed in the 1 $Kmin^{-1}$ measurement, but that is not the case.[32-34] Rather, SCO occurs without hysteresis under those conditions, in abrupt and gradual steps (Figure 1, bottom). That is consistent with the powder diffraction data, which were measured under "slow" conditions and show SCO in phase 2 occurs without significant structural changes. These observations could be explained if SCO in phase 2 in fact follows three kinetic regimes: fast, intermediate (both at 5 $Kmin^{-1}$) and slow (at 1 $Kmin^{-1}$). Such behavior could arise if phase 2 contains two unique switching centers, as in phase 1, which undergo SCO independently of each other. Be that as it may, the interplay between the processes is evidently complex, and further experiments to deconvolute the relationship between them are planned.[47]

Reverse-SCO can also be induced when a fraction of the sample is kinetically trapped in its high-spin form upon cooling. Rewarming that sample above its thermal relaxation temperature allows it to relax to its thermodynamic spin state population, leading to a complete or partial high→low-spin conversion on warming.[30,48] This is common upon thermal cycling of SCO occurring below *ca* 100 K, but is much rarer at higher temperatures.[49] Alternatively, order:disorder transitions in flexible ligand substituents can transfer entropy to a metal ion, thus triggering a reverse high→low-spin switching on warming. However, this only causes small perturbations to the magnetic susceptibility of iron(II) complexes, which have a high entropy penalty for reverse-SCO.[35,46] Hence, these other mechanisms are less likely to occur in phase 2.

A second novel aspect of **1[BF_4]$_2$**·x$MeNO_2$ is the incomplete nature of the spin-transition in phase 3. Incomplete SCO in phase-pure materials usually reflects the existence of separate active and inactive switching sites in the material, as in **1[BF_4]$_2$**·yMe_2CO below;[15,50] or kinetic trapping of a high-spin fraction of the sample at low temperatures (as above).[30,48] However, this is a rare example of incomplete SCO at a single metal site being imposed by intermolecular crystal packing.[41]

In contrast, **1[ClO_4]$_2$**·$MeNO_2$ and the two acetonitrile solvate salts show typical gradual thermal SCO, with $T_{½}$ = 244 (**1[ClO_4]$_2$**·$MeNO_2$), 276 (**1[BF_4]$_2$**·MeCN) and 253 K (**1[ClO_4]$_2$**·MeCN; Figure 5). These transitions are fully reversible after heating to 350 K. That is consistent with TGA data for the perchlorate salts, which both show an abrupt mass loss corresponding to 1 equiv solvent above 370-380 K.

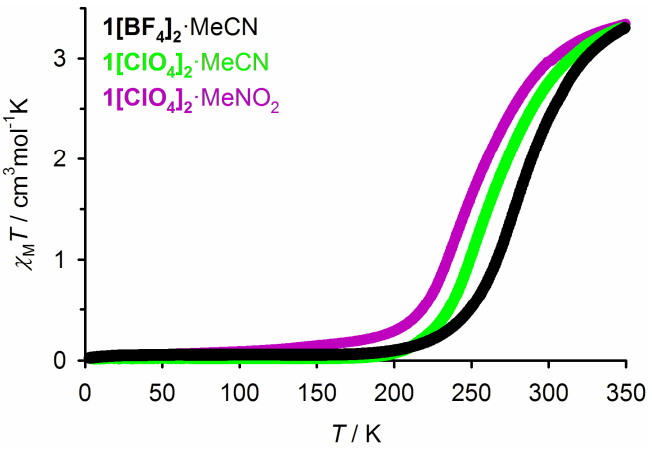

Figure 5 Magnetic susceptibility data for **1[ClO_4]$_2$**·$MeNO_2$, **1[BF_4]$_2$**·MeCN and **1[ClO_4]$_2$**·MeCN. Data were measured in cooling and warming temperature ramps, at a 5 $Kmin^{-1}$ scan rate.

Crystals of **1[ClO$_4$]$_2$**·MeNO$_2$ and **1[ClO$_4$]$_2$**·MeCN are isostructural at room temperature (both monoclinic, $P2_1/n$, Z = 4; phase 1), but undergo different symmetry-breaking transitions on cooling. The low-temperature phase 2 structure of **1[ClO$_4$]$_2$**·MeNO$_2$ is a racemic twin in the monoclinic $P2_1$ space group with Z = 4. Its unit cell parameters are very similar to those of phase 1, with the phase 1→2 transformation simply involving loss of the crystallographic *n* glide plane. In contrast phase 2 of **1[ClO$_4$]$_2$**·MeCN is triclinic, in $P\bar{1}$ with Z = 4. The unit cell parameters of this phase also resemble phase 1, with $a = a'$, $b = c'$, $c = b'$, $\alpha \approx \beta \approx 90°$ and $\gamma \approx \beta'$. Both these phase 2 structures contain two unique molecules per asymmetric unit.

The evolution of the complex's metric parameters in both solvates mirrors the spin-transition from their magnetic data (Figure S22). Variable temperature unit cell data show the phase 1→2 transitions occur at 160±10 K (**1[ClO$_4$]$_2$**·MeNO$_2$) and 215±15 K (**1[ClO$_4$]$_2$**·MeCN), when the materials are almost or fully low-spin (Figures S23-S26). Consistent with that, the two unique cation environments in both phase 2 structures are low-spin, with essentially identical metric parameters and ligand conformations at 120 K (Table S9). Rather, the symmetry breaking is induced by small displacements of the anions and solvent between the two phases.

The closest intermolecular contact between cations in phase 1 is a weak face-to-face π... π overlap between pyrazolyl rings, which associates the molecules into zig-zag chains along the [101] crystal vector in phase 1. These π... π contacts are retained in both phase 2 structures, with 'A' and 'B' cation sites alternating along the chains. The structures differ in the relative orientations of nearest neighbor π... π chains in the lattice. In phase 2 **1[ClO$_4$]$_2$**·MeNO$_2$, the A and B cations sites in neighboring chains along [010] have an 'all A' or 'all B' distribution, but alternate down the equivalent vector [001] in phase 2 **1[ClO$_4$]$_2$**·MeCN (Figure S20).

Two polymorphs with similar prismatic morphologies were isolated from samples of **1[BF$_4$]$_2$**·MeCN. The major polymorph consistently suffered from twinning, but a preliminary structure solution showed it to be isostructural with the triclinic phase 2 of **1[ClO$_4$]$_2$**·MeCN at 120 K. The other polymorph (monoclinic, *Pc*, Z = 4) was only detected in some crystallization vials, and is crystallographically unrelated to the perchlorate solvates. It contains two unique molecules in its asymmetric unit, which differ in the orientation of their S*t*Bu groups (Figure S27). Unusually, both molecules undergo abrupt SCO simultaneously at $T_{½}$ = 255 ±5 K, without a crystallographic phase change (Table S13).[51] That is inconsistent with the more gradual SCO in the magnetic data from this compound, however (Figure 5).

Both perchlorate solvates are single phase materials and are isostructural with their crystallographic phases, by X-ray powder diffraction at room temperature (Figure S30). However, the powder pattern of **1[BF$_4$]$_2$**·MeCN implies bulk samples of that material are isostructural to **1[ClO$_4$]$_2$**·MeCN, and the crystallographically characterized *Pc* polymorph is at most a minor component of the material (Figure S31). That explains the gradual thermal SCO exhibited by both acetonitrile solvate salts, as opposed to the abrupt spin-transition in the *Pc* phase.

The acetone solvates of the two salts are not isostructural, and show very different behaviors. Crystals of **1[BF$_4$]$_2$**·*y*Me$_2$CO (y ≈ 1.59; orthorhombic, $P2_12_12_1$, Z = 20, Z' = 5[36]) have a large unit cell and are sensitive to solvent loss, but a reasonably precise refinement was achieved at 120 K. Its asymmetric unit contains five unique complex cations, of which molecule A is high-spin; molecule B is predominantly, but not fully, low-spin; and molecules C-E are low-spin at that temperature (Figures S32-S33; Table 2). The high-spin nature of molecule A can be

Table 2. Selected bond distances and angular parameters for **1[BF$_4$]$_2$**·*y*Me$_2$CO at 120 K [Å, °, Å^3]. The atom numbering is the same as in Figure S10, with A-E suffixes denoting the different unique molecules (Figures S32-S33).[a]

	Molecule A	Molecule B	Molecule C	Molecule D	Molecule E
Fe(1)–N(2)	2.119(6)	1.951(7)	1.906(5)	1.901(5)	1.886(7)
Fe(1)–N(9)	2.164(7)	2.018(8)	1.966(6)	1.998(6)	1.951(8)
Fe(1)–N(14)	2.195(7)	1.961(11)	1.967(6)	1.962(6)	1.972(8)
Fe(1)–N(23)	2.110(6)	1.922(6)	1.914(5)	1.912(5)	1.894(7)
Fe(1)–N(30)	2.161(7)	2.006(7)	1.948(6)	1.971(5)	1.981(7)
Fe(1)–N(35)	2.202(7)	2.002(6)	1.966(6)	1.971(5)	1.969(7)
V_{Oh}	11.95(2)	9.89(2)	9.497(17)	9.614(17)	9.46(2)
Σ	156.2(8)	93.2(10)	87.3(8)	86.7(7)	90.2(10)
Θ	469	302	283	281	282
ϕ	158.2(2)	171.0(3)	175.8(3)	176.8(2)	177.3(3)
θ	83.57(8)	89.01(8)	89.20(7)	88.64(7)	85.28(9)

[a] V_{Oh}, Σ and Θ are indices showing the spin state of the complex,[42,43] while ϕ and θ measure the relative orientations of the two tridentate ligands in the molecule.[44,45] Typical values for these parameters in [Fe(bpp)$_2$]$^{2+}$ derivatives are given in refs. [6] and [8].

attributed to its molecular structure, which is significantly more distorted than the other cations. This is most notable in its *trans*-N{pyridyl}–Fe–N{pyridyl} angle (ϕ) of 158.2(2)°, which deviates strongly from the ideal value of 180°.[43] High-spin $[Fe(bpp)_2]^{2+}$ derivatives like $[FeL_2]^{2+}$ with $\phi < 165°$ rarely undergo SCO on cooling, being trapped in their high-spin form by the constraints of the surrounding lattice.[8,45,52] Since the energy penalty for this angular distortion is ≤1 kcal mol^{-1}, the greater structural distortion of molecule 'A' compared to molecules B-E is probably a packing effect, imposed by the surrounding lattice.[45,52,53]

Magnetic susceptibility data from freshly prepared crystals show the sample is *ca* 80 % high-spin ($\chi_M T$ = 2.8 cm^{3}mol^{-1}K) at 300 K and undergoes extremely gradual SCO on cooling, to a residual 30 % high-spin population ($\chi_M T$ = 1.1 cm^{3}mol^{-1}K) which remains constant below 100 K (Figure 6). The transformation occurs without hysteresis and in two discrete steps, centered near 150 and 275 K from the first derivative maxima in the data (Figure 6, inset). Warming above 330 K leads to a rapid drop in $\chi_M T$, corresponding to desolvation of the sample in the TGA data for the compound. The solvent-free material is amorphous by powder diffraction and, unusually, is fully low-spin. It's more common for desolvation of an SCO crystal to stabilize its high-spin form, as the complex expands in to the voids in the lattice.[38]

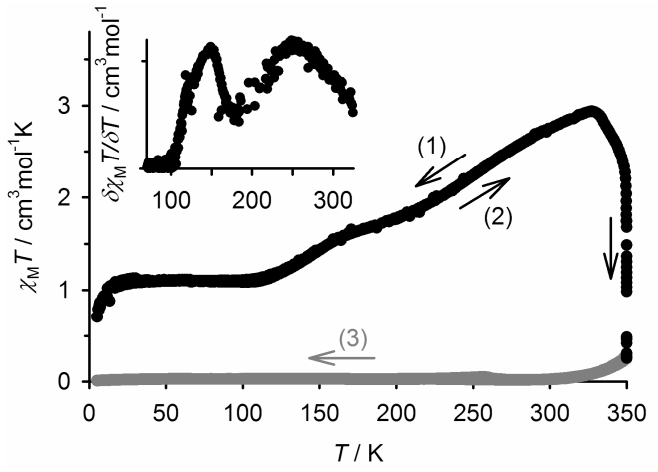

Figure 6 Magnetic susceptibility data for **1[BF$_4$]$_2$**·*y*Me$_2$CO on the thermal cycle: (1) 300→5 K; (2) 5→350 K; and (3) 350→5 K. Data were measured at a 5 Kmin^{-1} scan rate. The inset shows the first derivative of scans 1 and 2.

Although the plateau spin-state population below 100 K in the magnetic data (30 %) is slightly higher than predicted crystallographically (*ca* 25 % at 120 K), in other respects there is good agreement between the two techniques. Molecule A in the crystal remains high-spin; the SCO event around 150 K, which corresponds to *ca* 20 % of the sample ($\Delta\chi_M T$ = 0.7 cm^{3}mol^{-1}K), can be assigned to molecule B; while molecules C-E undergo SCO at higher temperature. A handful of materials are known to form high-*Z*' intermediate or product phases *via* crystallographic symmetry breaking during SCO.[37,54] However, **1[BF$_4$]$_2$**·*y*Me$_2$CO is a unique example of a high *Z*' crystal undergoing stepwise SCO without a crystallographic phase change.[55]

Lastly, the asymmetric unit of **1[ClO$_4$]$_2$**·0.5Me$_2$CO·0.2H$_2$O (triclinic, $P\bar{1}$, *Z* = 2) contains one unique cation site, with half an acetone molecule spanning the crystallographic inversion center (Figure S35). The complex is low-spin at room temperature, but shows the onset of a gradual, reversible SCO on heating. Annealing its single crystals at 370 K on the diffractometer causes loss of the acetone solvent, in a single-crystal-to-single-crystal transformation to a solvent-free phase with a three-fold expansion of the unit cell (triclinic, $P\bar{1}$, *Z* = 6). The three unique molecules in the annealed phase are all low-spin, but differ in the orientation of their *tert*butylsulfanyl groups (Table S14). One *t*BuS substituent in molecule 'B' of the desolvated phase has rotated about its C{pyridyl}–S bond by *ca* 60° compared to molecules A and C, which retain the ligand conformation in the original solvated form (Figure S36).

The solvent-free **1[ClO$_4$]$_2$** crystal contained solvent-accessible voids of 470 Å^3 per unit cell at 120 K, or 78 Å^3 per formula unit, which were essentially empty according to a *SQUEEZE* analysis.[56] However, they may account for the observation that bulk samples of **1[ClO$_4$]$_2$**·0.5Me$_2$CO·0.2H$_2$O absorb atmospheric moisture after annealing, leading to a microanalysis formulation of **1[ClO$_4$]$_2$**·2H$_2$O. Since the volume of a water molecule is 30 Å^3,[57] accommodation of two water molecules within the 78 Å^3 lattice voids is reasonable. Magnetic measurements show **1[ClO$_4$]$_2$**·2H$_2$O is also low-spin at room temperature and below. Desolvation of bulk samples of **1[ClO$_4$]$_2$**·0.5Me$_2$CO·0.2H$_2$O occurs cleanly with no loss of crystallinity, by X-ray powder diffraction (Figure S39).

Conclusions

The apparently simple solvate crystals formed by **1[BF$_4$]$_2$** and **1[ClO$_4$]$_2$** exhibit surprisingly complex spin state behaviors. Most unusual is the stepwise partial desolvation of **1[BF$_4$]$_2$**·*x*MeNO$_2$ from phase 1 (*x* = 2.3) to phase 3 (*x* = 0.75) *via* a detectable intermediate phase 2. Irreversible spin state changes coupled to structural transformations are common in SCO materials, and are usually (but not always[58]) triggered by loss of lattice solvent.[38,58] As in **1[BF$_4$]$_2$**·*x*MeNO$_2$, such changes may occur slowly over the timescale of a magnetic susceptibility measurement, and only proceed to completion over multiple thermal cycles.[58,59] However, two properties of **1[BF$_4$]$_2$**·*x*MeNO$_2$ are especially noteworthy: the involvement of an intermediate phase in the irreversible desolvation process;[60] and, the reverse-SCO component shown by phase 2 in the 5 Kmin^{-1} magnetic measurement (Figure 1). The latter feature has a kinetic origin, since it is not observed at a slower scan rate.

The magnetic data from phase 2 resemble other materials exhibiting different spin-transition regimes, which are linked *via* a structural transformation that is slow on the timescale of the measurement. At slower scan rates the structural change can proceed to completion during the measurement, so only the "slow" spin-transition should be observed.[32-34] However, Figure 1 implies the SCO kinetics in phase 2 are more complex than the literature examples, and may involve three distinct kinetic regimes. Since phase 2 was not crystallographically characterized, these observations cannot be explained in detail. However they become

more reasonable if phase 2 contains more than one structurally independent SCO switching site, as in phase 1. The SCO discontinuity at 50 % completeness in phase 2 at 1 $Kmin^{-1}$ lends tentative support to that suggestion.[61] In any case, the most likely origin of its slow transition kinetics are reorientation of a bulky *tert*butyl group or an order:disorder transition during SCO. Conformational changes involving the S*t*Bu substituents are involved in other structural transformations in this study, as discussed below.

The final phase 3 has another novel feature, of undergoing an abrupt spin-transition to 50 % completeness. Phase 3 contains one unique iron site with one *L* ligand disordered over two equally populated conformations. One of these half-occupied ligand sites is SCO-active while the other is not, which we attribute to the steric consequences of a BF_4^- ion in contact with the inactive disorder site. This is a rare example of incomplete SCO switching at a single iron center, which can be attributed to an individual intermolecular steric clash involving one of the spin states.[41]

Other noteworthy observations include **1[ClO$_4$]$_2$**·$MeNO_2$ and **1[ClO$_4$]$_2$**·MeCN, which exhibit almost identical gradual SCO (Figure 5) and are isostructural at room temperature, but transform to different low-temperature phases when the samples are fully low-spin. **1[BF$_4$]$_2$**·yMe_2CO contains five crystallographically unique molecules, four of which undergo very gradual SCO in two resolvable steps; this is the highest *Z*' crystal known to undergo SCO without a crystallographic phase change.[54] Although no spin-transition is involved, **1[ClO$_4$]$_2$**·0.5Me_2CO·0.2H_2O undergoes a single-crystal-single-crystal desolvation coupled to a crystallographic *Z*' = 1→3 symmetry breaking, involving rotation of a S*t*Bu substituent in one-third of the cations in the crystal. A similar S*t*Bu group reorientation might be involved in the phase transformations of **1[BF$_4$]$_2$**·*x*$MeNO_2$, as proposed above.

The variable *tert*butylsulfanyl group conformations in these compounds contrast with other related compounds. The S*t*Bu groups are perpendicular to the heterocyclic core in both phases of the free *L* ligand, and in **1[BF$_4$]$_2$**·*x*$MeNO_2$, with C{pyridyl}−C{pyridyl}−S−C{*t*Bu} torsions >70°. Conversely, the S*t*Bu groups are oriented almost parallel (coplanar) to their bound pyridyl rings in all the perchlorate solvate crystals. **1[BF$_4$]$_2$**·yMe_2CO and the structurally characterized phase of **1[BF$_4$]$_2$**·MeCN contain a mixture of perpendicular and parallel S*t*Bu conformations, while desolvation of **1[ClO$_4$]$_2$**·0.5Me_2CO·0.2H_2O involves rotation of a S*t*Bu group from a parallel towards a perpendicular orientation. In contrast, other 4-alkylsulfanyl-bpp derivatives and their iron complexes consistently adopt the "parallel" substituent conformation,[28-31] implying conjugation of the S atom lone pairs with the bpp pyridyl π-system.[62] The conformational variability in *L* and $[FeL_2]^{2+}$ reflects the greater steric bulk of the S*t*Bu substituent, which evidently contributes to the unusually complicated spin-state and crystal phase behavior in this system.

Experimental Section

Instrumentation

Solid state magnetic susceptibility measurements were performed with freshly isolated, unground polycrystalline samples, using a Quantum Design MPMS-3 SQUID/VSM magnetometer in an applied field of 5000 G. Unless otherwise specified, the measurements employed a temperature ramp of 5 $Kmin^{-1}$. Diamagnetic corrections for the samples were estimated from Pascal's constants;[63] a previously measured diamagnetic correction for the sample holder was also applied to the data. Solvated samples were protected against solvent loss by saturating the (tightly sealed) sample holder capsules with a drop of diethyl ether. Different samples from the same crystallization vials were used for the thermogravimetric analyses, which employed a TA Instruments TGA Q50 analyser with a temperature ramp of 10 $Kmin^{-1}$ under a stream of nitrogen gas. Room temperature X-ray powder diffraction measurements were obtained from a Bruker D2 Phaser diffractometer, while variable temperature powder diffraction data were obtained from a Bruker D8 Advance A25 instrument. Both powder diffractometers employed Cu K_α radiation (λ = 1.5418 Å).

Elemental microanalyses were performed by the London Metropolitan University School of Human Sciences microanalytical service. Electrospray mass spectra (ESMS) were obtained on a Bruker MicroTOF spectrometer, from MeCN feed solutions. All mass peaks have the correct isotopic distributions for the proposed assignments. NMR spectra were obtained using a Bruker Avance 500 FT spectrometer operating at 500.1 MHz (^{1}H) or 125 MHz (^{13}C).

Materials and methods

Unless otherwise stated, all reactions were carried out in air using as-supplied AR-grade solvents. All reagents and solvents were purchased commercially and used as supplied.

Synthesis of 4-(*tert*butylsulfanyl)-2,6-di(pyrazol-1-yl)-pyridine (*L*). Sodium 2-methyl-2-propanethiolate (5 g, 45 mmol) was added to a solution of 2,4,6-trifluoropyridine (5.9 g, 45 mmol) in tetrahydrofuran (60 cm^3) at ambient temperature. After stirring for 10 mins, solid pyrazole (6.74 g, 99 mmol) and sodium hydride (60 wt % in mineral oil; 4.3 g, 110 mmol) were added in that order. After the effervescence ceased, the suspension was stirred for additional 4 hr at 50 °C. All volatiles were then removed using reduced pressure. The residue was washed with hexane and all washings combined and concentrated. Flash silica column chromatography (2:1 dichloromethane:hexane eluent) afforded *L* as a pale yellow oil (R_f 0.15), which slowly crystallized upon standing at room temperature. Yield 0.80 g, 6 % yield. ESMS *m/z* 244.0653 (calcd for $[HL-C\{CH_3\}_3]^+$ 244.0651), 300.1294 (calcd for $[HL]^+$ 300.1277), 322.1105 (calcd for $[NaL]^+$ 322.1097), 621.2309 (calcd for $[NaL]^+$ 621.2302). ^{1}H NMR ($CDCl_3$) δ 1.51 (s, 9H, $C(CH_3)_3$), 6.50 (dd, 1.7 and 2.4 Hz, 2H, Pz H^4), 7.77 (d, 1.7 Hz, 2H, Pz H^3), 7.97 (s, 2H, Py $H^{3/5}$), 8.56 (d, 2.4 Hz, 2H, Pz H^5). ^{13}C NMR ($CDCl_3$) δ 31.4 (3C, $C(CH_3)_3$), 47.8 (1C, $C(CH_3)_3$), 108.0 (2C, Pz C^4), 113.6 (2C, Py $C^{3/5}$), 127.2 (2C, Pz C^5), 142.5 (2C, Pz C^3), 149.7 (2C, Py $C^{2/6}$), 151.3 (1C, Py C^4).

Synthesis of the complexes. The following method, described for **1[BF$_4$]$_2$**, was followed in each case. Solutions of *L* (100 mg, 0.33 mmol) and $Fe[BF_4]_2{\cdot}6H_2O$ (56 mg, 0.17 mmol) in nitromethane (2x 5 cm^3) were combined, leading to immediate formation of a yellow-brown colour. Addition of excess diethyl ether afforded an orange powder, which was collected and dried. Yield 107 mg, 76 %. ^{1}H NMR (CD_3NO_2) δ 1.5 (9H, $C(CH_3)_3$), 38.6 and 39.4 (both 4H, Pz H^3 and Py $H^{3/5}$), 57.8 (4H, Pz H^4), 66.5 (4H, Pz H^5).

Recrystallization of **1[BF$_4$]$_2$** by slow diffusion of diethyl ether into solutions of the complex in the appropriate solvent yielded the different solvate materials described below. Solvates of yellow **1[ClO$_4$]$_2$** were prepared similarly, using $Fe[ClO_4]_2{\cdot}6H_2O$ (62 mg, 0.17 mmol) as the metal salt reagent.

Elemental analysis for **1[BF$_4$]$_2$·2.34MeNO$_2$** (phase 1): Calcd (%) for $C_{30}H_{34}B_2F_8FeN_{10}S_2{\cdot}2.34CH_3NO_2$ (971.07): C 40.0, H 4.26, N 17.8; found: C 39.8, H 4.31, N 17.2. After drying *in vacuo* at 80 °C for 16 hrs, followed by exposure to air, the same crystals analysed with a formulation consistent with phase 3 of the material. Elemental analysis for **1[BF$_4$]$_2$·¾MeNO$_2$** (phase 3): Calcd (%) for $C_{30}H_{34}B_2F_8FeN_{10}S_2{\cdot}¾CH_3NO_2$ (889.29): C 42.3, H 4.18, N 17.2. Found: C 41.8, H 4.11, N 17.3.

Elemental analysis for **1[BF$_4$]$_2$·MeCN**: Calcd (%) for $C_{30}H_{34}B_2F_8FeN_{10}S_2{\cdot}CH_3CN$ (869.31): C 44.2, H 4.29, N 17.7; found: C 44.1, H 4.34, N 17.6.

Elemental analysis for **1[BF$_4$]$_2$·½Me$_2$CO·H$_2$O**: Calcd (%) for $C_{30}H_{34}B_2F_8FeN_{10}S_2{\cdot}½Me_2CO{\cdot}H_2O$ (875.1): C 43.2, H 4.49, N 16.0; found: C 43.1, H 4.23, N 15.8. After drying *in vacuo* at 80 °C for 16 hrs, followed by exposure to air, the same crystals analysed with a monohydrate formulation. Elemental analysis for **1[BF$_4$]$_2$·H$_2$O**: Calcd (%) $C_{30}H_{34}B_2F_8FeN_{10}S_2{\cdot}H_2O$ (846.37): C 42.6, H 4.29, N 16.6; found: C 42.5, H 4.14, N 16.5.

Elemental analysis for **1[ClO$_4$]$_2$·MeNO$_2$**: Calcd (%) for $C_{30}H_{34}Cl_2FeN_{10}O_8S_2{\cdot}CH_3NO_2$ (914.58): C 40.7, H 4.08, N 16.9; found: C 40.8, H 4.12, N 16.8.

Elemental analysis for **1[ClO$_4$]$_2$·MeCN**: Calcd (%) for $C_{30}H_{34}Cl_2FeN_{10}O_8S_2{\cdot}CH_3CN$ (894.60): C 43.0, H 4.17, N 17.2; found: C 42.9, H 4.26, N 17.2.

Elemental analysis for **1[ClO$_4$]$_2$·½Me$_2$CO·*n*H$_2$O** (phase 1; *n* = 0,5): Calcd (%) for $C_{30}H_{34}Cl_2FeN_{10}O_8S_2{\cdot}½Me_2CO{\cdot}½H_2O$ (891.58): C 42.4, H 4.30, N 15.7; found: C 42.0, H 4.17, N 15.6. After drying *in vacuo* at 80 °C for 16 hrs, followed by exposure to air, the same sample gave a microanalysis consistent with a dihydrate material. Elemental analysis for **1[ClO$_4$]$_2$·2H$_2$O**: Calcd (%) $C_{30}H_{34}Cl_2FeN_{10}O_8S_2{\cdot}2H_2O$ (889.57): C 40.5, H 4.31, N 15.8; found: C 40.4, H 3.92, N 15.6.

Single-crystal structure analyses

The two polymorphs of *L* crystallized together from the oil that was initially obtained after purification of the compound. Crystals of each **1[BF$_4$]$_2$**·solv and **1[ClO$_4$]$_2$**·solv material were prepared as described above, except for the following samples. The crystal of phase 3 of **1[BF$_4$]$_2$**·*x*MeNO$_2$ was found in a sample of the compound which had been annealed inside the SQUID magnetometer. Heating a crystal of phase 1 of **1[ClO$_4$]$_2$**·½Me$_2$CO·*n*H$_2$O at 370 K for 30 mins on the diffractometer transformed it into solvent-free phase 2, in single-crystal-to-single-crystal fashion. Where applicable, the same crystal was used for data collections at multiple temperatures.

All diffraction data were collected with an Agilent Supernova dual source diffractometer using monochromated Cu-K_α radiation (λ = 1.54184 Å). Experimental details of the structure determination of each compound and full details of all the crystallographic refinements, are given in the Supporting Information (Tables S1-S6). The structures were solved by direct methods (*SHELXS97*),[64] and developed by full least-squares refinement on F 2 *(SHELXL97*).[64] Crystallographic figures were prepared using *X-SEED*,[65] and structural parameters in Tables 1 and 2 and the Supporting Information[42,44] were calculated with *Olex 2*.[66]

Acknowledgements

This work was funded by the EPSRC (EP/K012576/1 and EP/N509681/1). We thank Dr Christopher Pask (University of Leeds) for assistance during the preparation of the manuscript.

Keywords: spin-crossover • iron • N-ligands • symmetry breaking • X-ray diffraction.

[1] *Spin Crossover in Transition Metal Compounds I–III, Top. Curr. Chem.* (Eds.: P. Gütlich, H. A. Goodwin), Springer, New York, **2004**, vols. 233–235.

[2] M. A. Halcrow (ed), *Spin-crossover materials – properties and applications,* John Wiley & Sons, Chichester, UK, **2013**, p. 568.

[3] J. Zarembowitch, F. Varret, A. Hauser, J. A. Real, K. Boukheddaden, *C. R. Chimie* **2018**, *21*, 1056–1059.

[4] a) K. S. Kumar, M. Ruben, *Coord. Chem. Rev.* **2017**, *346*, 176–205; b) S. Rat, M. Piedrahita-Bello, L. Salmon, G. Molnár, P. Demont, A. Bousseksou, *Adv. Mater.* **2018**, *30*, 1703862.

[5] a) O. Kahn, J. Krober, C. Jay, *Adv. Mater.* **1992**, *4*, 718–728; b) M. D. Manrique-Juárez, S. Rat, L. Salmon, G. Molnár, C. M. Quintero, L. Nicu, H. J. Shepherd, A. Bousseksou, *Coord. Chem. Rev.* **2016**, *308*, 395–408; c) G. M. Espallargas, E. Coronado, *Chem. Soc. Rev.* **2018**, *47*, 533–557.

[6] M. A. Halcrow, *Chem. Soc. Rev.* **2011**, *40*, 4119–4142

[7] M. Chergui, E. Collet, *Chem. Rev.* **2017**, *117*, 11025−11065.

[8] M. A. Halcrow, *Coord. Chem. Rev.* **2009**, *253*, 2493–2514

[9] a) J. Olguín, S. Brooker, *Coord. Chem. Rev.* **2011**, *255*, 203–240; b) L. J. Kershaw Cook, R. Mohammed, G. Sherborne, T. D. Roberts, S. Alvarez, M. A. Halcrow, *Coord. Chem. Rev.* **2015**, *289–290*, 2–12.

[10] M. Attwood, S. S. Turner, *Coord. Chem. Rev.* **2017**, *353*, 247–277.

[11] a) R. González-Prieto, B. Fleury, F. Schramm, G. Zoppellaro, R. Chandrasekar, O. Fuhr, S. Lebedkin, M. Kappes, M. Ruben, *Dalton Trans.* **2011**, *40*, 7564–7570; b) A. Santoro, L. J. Kershaw Cook, R. Kulmaczewski, S. A. Barrett, O. Cespedes, M. A. Halcrow, *Inorg. Chem.* **2015**, *54*, 682–693.

[12] B. Schäfer, T. Bauer, I. Faus, J. A. Wolny, F. Dahms, O. Fuhr, S. Lebedkin, H.-C. Wille, Kai Schlage, K. Chevalier, F. Rupp, R. Diller, V. Schünemann, M. M. Kappes, M. Ruben, *Dalton Trans.* **2017**, *46*, 2289–2302.

[13] K. S. Kumar, I. Šalitroš, N. Suryadevara, E. Moreno-Pineda, M. Ruben, *Eur. J. Inorg. Chem.* **2018**, 5091–5097.

[14] K. Takahashi, Y. Hasegawa, R. Sakamoto, M. Nishikawa, S. Kume, E. Nishibori, H. Nishihara, *Inorg. Chem.* **2012**, *51*, 5188−5198.

[15] I. Šalitroš, R. Herchel, O. Fuhr, R. González-Prieto, M. Ruben, *Inorg. Chem.* **2019**, *58*, 4310−4319.

[16] M. Nihei, L. Han, H. Oshio, *J. Am. Chem. Soc.* **2007**, *129*, 5312−5313.

[17] M. Nihei, N. Takahashi, H. Nishikawa, H. Oshio, *Dalton Trans.* **2011**, *40*, 2154–2156.

[18] A. Abhervé, M. Palacios-Corella, J. M. Clemente-Juan, R. Marx, P. Neugebauer, J. van Slageren, M. Clemente-León, E. Coronado, *J. Mater. Chem. C* **2015**, *3*, 7936−7945.

[19] A. Abhervé, M. J. Recio-Carretero, M. López-Jordà, J. M. Clemente-Juan, J. Canet-Ferrer, A. Cantarero, M. Clemente-León, E. Coronado, *Inorg. Chem.* **2016**, *55*, 9361−9367.

[20] I. Galadzhun, R. Kulmaczewski, O. Cespedes, M. Yamada, N. Yoshinari, T. Konno, M. A. Halcrow, *Inorg. Chem.* **2018**, *57*, 13761−13771.

[21] a) A. K. Botcha, S. Basak, R. Chandrasekar, *RSC Adv.* **2014**, *4*, 34760–34763; b) K. S. Kumar, I. Šalitroš, B. Heinrich, S. Moldovan, M. Mauro, M. Ruben, *J. Phys.: Condens. Matter* **2020**, *32*, 204002.

[22] a) E. J. Devid, P. N. Martinho, M. V. Kamalakar, I. Šalitroš, Ú. Prendergast, J.-F. Dayen, V. Meded, T. Lemma, R. González-Prieto, F. Evers, T. E. Keyes, M. Ruben, B. Doudin, S. J. van der Molen, *ACS Nano* **2015**, *9*, 4496–4507; b) K. S. Kumar, I. Šalitroš, Z. Boubegtiten-Fezoua, S. Moldovan, P. Hellwig, M. Ruben, *Dalton Trans.* **2018**, *47*, 35–40; c) E.

Burzurí, A. García-Fuente, V. García-Suárez, K. S. Kumar, M. Ruben, J. Ferrer, H. S. J. van der Zant, *Nanoscale* **2018**, *10*, 7905–7911.

[23] L. Pukenas, F. Benn, E. Lovell, A. Santoro, L. J. Kershaw Cook, M. A. Halcrow, S. D. Evans, *J. Mater. Chem. C* **2015**, *3*, 7890−7896.

[24] a) C. Rajadurai, O. Fuhr, R. Kruk, M. Ghafari, H. Hahn, M. Ruben, *Chem. Commun.* **2007**, 2636–2638; b) C. A. Tovee, C. A. Kilner, S. A. Barrett, J. A. Thomas, M. A. Halcrow, *Eur. J. Inorg. Chem.* **2010**, 1007–1012; c) I. Capel Berdiell, R. Kulmaczewski, S. L. Warriner, O. Cespedes, M. A. Halcrow, *Eur. J. Inorg. Chem.*, doi: 10.1002/ejic.202000782.

[25] L. J. Kershaw Cook, J. Fisher, L. P. Harding, M. A. Halcrow, *Dalton Trans.* **2015**, *44*, 9417–9425.

[26] L. J. Kershaw Cook, R. Kulmaczewski, R. Mohammed, S. Dudley, S. A. Barrett, M. A. Little, R. J. Deeth, M. A. Halcrow, *Angew. Chem. Int. Ed.* **2016**, *55*, 4327–4331; *Angew. Chem.* **2016**, *128*, 4399–4403.

[27] M. A. Halcrow, I. Capel Berdiell, C. M. Pask, R. Kulmaczewski, *Inorg. Chem.* **2019**, *58*, 9811−9821.

[28] a) L. J. Kershaw Cook, H. J. Shepherd, T. P. Comyn, C. Baldé, O. Cespedes, G. Chastanet, M. A. Halcrow, *Chem. Eur. J.* **2015**, *21*, 4805–4816; b) L. J. Kershaw Cook, R. Kulmaczewski, S. A. Barrett, M. A. Halcrow, *Inorg. Chem. Front.* **2015**, *2*, 662–670.

[29] L. J. Kershaw Cook, R. Kulmaczewski, O. Cespedes, M. A. Halcrow, *Chem. Eur. J.* **2016**, *22*, 1789–1799.

[30] R. Kulmaczewski, E. Trzop, L. J. Kershaw Cook, E. Collet, G. Chastanet, M. A. Halcrow, *Chem. Commun.* **2017**, *53*, 13268–13271.

[31] R. Kulmaczewski, E. Trzop, E. Collet, S. Vela, M. A. Halcrow, *J. Mater. Chem. C* **2020**, *8*, 8420–8429.

[32] a) S. Hayami, Z.-z. Gu, Y. Einaga, Y. Kobayasi, Y. Ishikawa, Y. Yamada, A. Fujishima, O. Sato, *Inorg. Chem.* **2001**, *40*, 3240–3242; b) J. S. Costa, P. Guionneau, J.-F. Létard, *J. Phys. Conf. Ser.* **2005**, *21*, 67–72; c) P. Guionneau, F. Le Gac, A. Kaiba, J. S. Costa, D. Chasseau, J.-F. Létard, *Chem. Commun.* **2007**, 3723–3725; d) H. Wang, C. Baldé, A. Grosjean, C. Desplanches, P. Guionneau, G. Chastanet, *Dalton Trans.* **2018**, *47*, 14741–14750.

[33] a) M. Seredyuk, M. C. Muñoz, M. Castro, T. Romero-Morcillo, A. B. Gaspar, J. A. Real, *Chem. Eur. J.* **2013**, *19*, 6591–6596; b) T. Delgado, A. Tissot, L. Guénée, A. Hauser, F. J. Valverde-Muñoz, M. Seredyuk, J. A. Real, S. Pillet, E. Bendeif, C. Besnard, *J. Am. Chem. Soc.* **2018**, *140*, 12870–12876; c) F. J. Valverde-Muñoz, M. Seredyuk, M. Meneses-Sánchez, M. C. Muñoz, C. Bartual-Murguia, J. A. Real, *Chem. Sci.* **2019**, *10*, 3807–3816.

[34] M. Weselski, M. Książek, D. Rokosz, A. Dreczko, J. Kusz, R. Bronisz, *Chem. Commun.* **2018**, *54*, 3895–3898

[35] a) P. Manikandan, K. Padmakumar, K. R. J. Thomas, B. Varghese, H. Onodera, P. T. Manoharan, *Inorg. Chem.* **2001,** *40,* 6930–6939; b) M. Seredyuk, A. B. Gaspar, V. Ksenofontov, Y. Galyametdinov, J. Kusz, P. Gütlich, *Adv. Funct. Mater.* **2008**, *18*, 2089–2101; c) M. Ostermeier, M.-A. Berlin, R. M. Meudtner, S. Demeshko, F. Meyer, C. Limberg, S. Hecht, *Chem. Eur. J.* **2010**, *16*, 10202–10213; d D. Rosario-Amorin, P. Dechambenoit, A. Bentaleb, M. Rouzières, C. Mathonière, R. Clérac, *J. Am. Chem. Soc.* **2018**, *140*, 98–101; e) M. Weselski, M. Książek, P. Mess, J. Kusz, R. Bronisz, *Chem. Commun.* **2019**, *55*, 7033–7036.

[36] K. M. Steed, J. W. Steed, *Chem. Rev.* **2015**, *115*, 2895–2933.

[37] a) M. Shatruk, H. Phan, B. A. Chrisostomo, A. Suleimenova, *Coord. Chem. Rev.* **2015**, *289–290*, 62–73; b) N. Ortega-Villar, M. C. Muñoz, J. A. Real, *Magnetochemistry* **2016**, *2*, 16.

[38] See *eg* a) Y. Garcia, P. J. Van Koningsbruggen, E. Codjovi, R. Lapouyade, O. Kahn, L. Rabardel, *J. Mater. Chem.* **1997**, *7*, 857–858; b) S. Hayami, Z.-Z. Gu, H. Yoshiki, A. Fujishima, O. Sato, *J. Am. Chem. Soc.* **2001**, *123*, 11644–11650; c) C. Faulmann, K. Jacob, S. Dorbes, S. Lampert, I. Malfant, M.-L. Doublet, L. Valade, J. A. Real, *Inorg. Chem.* **2007**, *46*, 8548–8559; d) M. Clemente-León, E. Coronado, M. C. Giménez-López, F. M. Romero, *Inorg. Chem.* **2007**, *46*, 11266–11276; e) J. J. M. Amoore, S. M. Neville, B. Moubaraki, S. S. Iremonger, K. S. Murray, J.-F. Létard, C. J. Kepert, *Chem. Eur. J.* **2010**, *16*, 1973– 1982; f) T. D. Roberts, F. Tuna, T. L. Malkin, C. A. Kilner, M. A. Halcrow, *Chem. Sci.* **2012**, *3*, 349–354; g) A. Lennartson, P. Southon, N. F. Sciortino, C. J. Kepert, C. Frandsen, S. Mørup, S. Piligkos, C. J. McKenzie, *Chem. Eur. J.* **2015**, *21*, 16066–16072; h) W. Phonsri, C. G. Davies, G. N. L. Jameson, B. Moubaraki, K. S. Murray, *Chem. Eur. J.* **2016**, *22*, 1322–1333.

[39] Zero-field splitting of the residual high-spin material causes a further reduction in $\chi_M T$ at the lowest temperatures. R. Boča, *Coord. Chem. Rev.* **2004**, *248*, 757–815.

[40] Conversion of phase 2 to phase 3 is sluggish by powder diffraction and TGA (Figures 3 and S6), and it can be hard to reproduce *in situ* desolvation reactions inside the sealed powder sample capsules of the MPMS-3 magnetometer. Additional measurements of phase 2 at intermediate scan rates were not attempted, because of insufficient instrument time on the SQUID magnetometer.

[41] J. Elhaïk, C. A. Kilner, M. A. Halcrow, *CrystEngComm* **2005**, *7*, 151–157.

[42] V_{Oh} is the volume of the octahedron defined by the FeN_6 coordination sphere.[43] Σ is a general measure of the deviation of a metal ion from an ideal octahedral geometry, while Θ more specifically indicates its distortion towards a trigonal prismatic structure. Σ and Θ are usually larger in the high-spin than in the low-spin state, especially for complexes of chelating ligands with restricted bite angles like **1X₂**; a perfectly octahedral complex gives $\Sigma = \Theta = 0$.[43] Full definitions of Σ and Θ are in the Supporting Information.

[43] P. Guionneau, M. Marchivie, G. Bravic, J.-F. Létard, D. Chasseau, *Top. Curr. Chem.* **2004**, *234*, 97–128.

[44] θ is the dihedral angle between the least squares planes of the two *L* ligands, and ϕ is the *trans*-N{pyridyl}–Fe–N{pyridyl} bond angle [N(2)–Fe(1)–N(23) in Fig. 2)].[45] An ideal D_{2d}-symmetric geometry for a $[FeL_2]^{2+}$ center gives θ = 90 and ϕ = 180°, but many high-spin $[Fe(bpp)_2]^{2+}$ derivatives exhibit significantly reduced values for these parameters.[6,8] See the Supporting Information for more details.

[45] J. M. Holland, J. A. McAllister, C. A. Kilner, M. Thornton-Pett, A. J. Bridgeman, M. A. Halcrow, *J. Chem. Soc. Dalton Trans.* **2002**, 548–554.

[46] Reverse-SCO coupled to solid state order:disorder transitions has a stronger effect on the spin states of cobalt(II) compounds, whose entropy of SCO is smaller than for iron(II) materials. a) S. Hayami, M. R. Karim, Y. H. Lee, *Eur. J. Inorg. Chem.* **2013**, 683–696; b) R. G. Miller, S. Narayanaswamy, J. L. Tallon, S. Brooker., *New J. Chem.* **2014**, *38*, 1932–1941.

[47] An alternative interpretation might be if the processes in Figure 1 represent different stages in the desolvation of $\mathbf{1[BF_4]_2}\cdot x\mathrm{MeNO_2}$ during its conversion from phase 2 to phase 3. However, that seems unlikely since the "slow" non-hysteretic transition occurs cleanly in the 1 $Kmin^{-1}$ measurement, and is not an observable intermediate in the conversion of phase 2 to phase 3 at 5 $Kmin^{-1}$.

[48] See *eg* a) M. Marchivie, P. Guionneau, J.-F. Létard, D. Chasseau, J. A. K. Howard, *J. Phys. Chem. Solids* **2004**, *65*, 17–23; b) J.-F. Létard, S. Asthana, H. J. Shepherd, P. Guionneau, A. E. Goeta, N. Suemura, R. Ishikawa, S. Kaizaki, *Chem. Eur. J.* **2012**, *18*, 5924–5934; c) N. Paradis, G. Chastanet, J.-F. Létard, *Eur. J. Inorg. Chem.* **2012**, 3618-3624; d) G. A. Craig, J. S. Costa, S. J. Teat, O. Roubeau, D. S. Yufit, J. A. K. Howard, G. Aromí, *Inorg. Chem.* **2013**, *52*, 7203−7209; e) K. D. Murnaghan, C. Carbonera, L. Toupet, M. Griffin, M. M. Dîrtu, C. Desplanches, Y. Garcia, E. Collet, J.-F. Létard, G. G. Morgan, *Chem. Eur. J.* **2014**, *20*, 5613−5618; f) N. Paradis, G. Chastanet, T. Palamarciuc, P. Rosa, F. Varret, K. Boukheddaden, J.-F. Létard, *J. Phys. Chem. C* **2015**, *119*, 20039−20050.

[49] V. Gómez, C. Sáenz de Pipaón, P. Maldonado-Illescas, J. C. Waerenborgh, E. Martin, J. Benet-Buchholz, J. R. Galán-Mascarós, *J. Am. Chem. Soc.* **2015**, *137*, 11924−11927.

[50] a) R. Hinek, H. Spiering, D. Schollmeyer, P. Gütlich, A. Hauser, *Chem. Eur. J.* **1996**, *2*, 1427–1434; b) D. L. Reger, C. A. Little, V. G. Young, Jr., M. Pink, *Inorg. Chem.* **2001**, *40*, 2870–2874; c) J. Elhaïk, C. A. Kilner, M. A. Halcrow, *Dalton Trans.* **2006**, 823–830; d) R. Pritchard, S. A. Barrett, C. A. Kilner, M. A. Halcrow, *Dalton Trans.* **2008**, 3159–3168 and **2009**, 10622 (correction); e) A. Kaiba, H. J. Shepherd, D. Fedaoui, P. Rosa, A. E. Goeta, N. Rebbani, J.-F. Létard, P. Guionneau, *Dalton Trans.* **2010**,

39, 2910–2918; f) D. J. Harding, D. Sertphon, P. Harding, K. S. Murray, B. Moubaraki, J. D. Cashion, H. Adams, *Chem. Eur. J.* **2013**, *19*, 1082–1090; g) E. Milin, V. Patinec, S. Triki, E. Bendeif, S. Pillet, M. Marchivie, G. Chastanet, K. Boukheddaden, *Inorg. Chem.* **2016,** *55*, 11652–11661; h) M. A. Al-Azzani, F. Al-Mjeni, R. Mitsuhashi, M. Mikuriya, I. A. Al-Omari, C. C. Robertson, E. Bill, M. S. Shongwe, *Chem. Eur. J*. **2020**, *26*, 4766–4779.

[51] A. Lennartson, A. D. Bond, S. Piligkos, C. J. McKenzie, *Angew. Chem. Int. Ed.* **2012**, *51*, 11049–11052; *Angew. Chem.* **2012**, *124*, 11211–11214.

[52] S. Vela, J. J. Novoa, J. Ribas-Arino, *Phys. Chem. Chem. Phys.* **2014**, *16*, 27012–27024.

[53] I. Capel Berdiell, R. Kulmaczewski, M. A. Halcrow, *Inorg. Chem.* **2017**, *56*, 8817−8828.

[54] For molecular crystals that transform to intermediate or product phases with *Z'* ≥ 4 during SCO, see ref. [51] and: a) N. Bréfuel, E. Collet, H. Watanabe, M. Kojima, N. Matsumoto, L. Toupet, K. Tanaka, J.-P. Tuchagues, *Chem. Eur. J.* **2010**, *16*, 14060–14068; b) Z.-Y. Li, J.-W. Dai, Y. Shiota, K. Yoshizawa, S. Kanegawa, O. Sato, *Chem. Eur. J.* **2013**, *19*, 12948–12952; c) K. D. Murnaghan, C. Carbonera, L. Toupet, M. Griffin, M. M. Dîrtu, C. Desplanches, Y. Garcia, E. Collet, J.-F. Létard, G. G. Morgan, *Chem. Eur. J.* **2014**, *20*, 5613–5618; d) Z.-Y. Li, H. Ohtsu, T. Kojima, J.-W. Dai, T. Yoshida, B. K. Breedlove, W.-X. Zhang, H. Iguchi, O. Sato, M. Kawano, M. Yamashita, *Angew. Chem. Int. Ed.* **2016**, *55*, 5184–5189; *Angew. Chem.* **2016**, *128*, 5270–5275; e) R. Kulmaczewski, O. Cespedes, M. A. Halcrow, *Inorg. Chem.* **2017**, *56*, 3144−3148; f) I. Capel Berdiell, R. Kulmaczewski, O. Cespedes, M. A. Halcrow, *Chem. Eur. J.* **2018**, *24*, 5055–5059; g) T. Nakanishi, Y. Hori, S. Wu, H. Sato, A. Okazawa, N. Kojima, Y. Horie, H. Okajima, A. Sakamoto, Y. Shiota, K. Yoshizawa, O. Sato, *Angew. Chem. Int. Ed.* **2020**, *59*, 14781–14787; *Angew. Chem.* **2020**, *132*, 14891–14897.

[55] For molecular crystals with *Z'* ≥ 2 which are known to undergo complete or partial SCO without a crystallographic phase change, see ref. [51] and: a) J. Kusz, H. Spiering, P. Gütlich, *J. Appl. Cryst.* **2001**, *34*, 229–238; b) M. S. Shongwe, B A. Al-Rashdi, H. Adams, M. J. Morris, M. Mikuriya, G. R. Hearne, *Inorg. Chem*. **2007**, *46*, 9558–9568; c) R. Pritchard, S. A. Barrett, C. A. Kilner, M. A. Halcrow, *Dalton Trans*. **2008**, 3159–3168 and **2009**, 10622 (correction); d) M. A. Al-Azzani, F. Al-Mjeni, R. Mitsuhashi, M. Mikuriya, I. A. Al-Omari, C. C. Robertson, E. Bill, M. S. Shongwe, *Chem. Eur. J.* **2020**, *26*, 4766–4779.

[56] A. L. Spek, *Acta Cryst. Sect. C Struct. Chem.* **2015**, *71*, 9−18.

[57] One litre of water contains 55.6 moles, so the volume of one water molecule is 2.99 x10^{-26} dm^3, or 29.9 $Å^3$.

[58] a) V. Niel, M. C. Muñoz, A. B. Gaspar, A. Galet, G. Levchenko, J. A. Real, *Chem. Eur. J.* **2002**, *8*, 2446–2453; b) M. Książek, M. Weselski, A. Dreczko, V. Maliuzhenko, M. Kaźmierczak, A. Tołoczko, J. Kusz, R. Bronisz, *Dalton Trans*. **2020**, *49*, 9811–9819.

[59] a) M. B. Bushuev, V. A. Daletsky, D. P. Pishchur, Y. V. Gatilov, I. V. Korolkov, E. B. Nikolaenkova, V. P. Krivopalov, *Dalton Trans.* **2014**, *43*, 3906–3910; b) F.-L. Yang, X. Chen, W.-H. Wu, J.-H. Zhang, X.-M. Zhao, Y.-H. Shia, F. Shen, *Dalton Trans*. **2019**, *48*, 231–241; c) W.-Q. Gao, Y.-S. Meng, C.-H. Liu, Y. Pan, T. Liu, Y.-Y. Zhu, *Dalton Trans.* **2019**, *48*, 6323–6327.

[60] G. Aromí, C. M. Beavers, J. S. Costa, G. A. Craig, G. M. Espallargas, A. Orera, O. Roubeau, *Chem. Sci.* **2016**, *7*, 2907−2915.

[61] a) M. S. Shongwe, B. A. Al-Rashdi, H. Adams, M. J. Morris, M. Mikuriya, G. R. Hearne, *Inorg. Chem*. **2007**, *46*, 9558−9568; b) B. Weber, C. Carbonera, C. Desplances, J.-F. Létard, *Eur. J. Inorg. Chem.* **2008**, 1589–1598; c) W. Phonsri, D. J. Harding, P. Harding, K. S. Murray, B. Moubaraki, I. A. Gass, J. D. Cashion, G. N. L. Jameson, H. Adams, *Dalton Trans*. **2014**, *43*, 17509–17518; d) R. Díaz-Torres, W. Phonsri, K. S. Murray, L. Liu, M. Ahmed, S. M. Neville, P. Harding, D. J. Harding, *Inorg. Chem.* **2020**, *59*, 13784−13791; e) S. Chorazy, T. Charytanowicz, D. Pinkowicz, J. Wang, K. Nakabayashi, S. Klimke, F. Renz, S. Ohkoshi, B. Sieklucka, *Angew. Chem. Int. Ed.* **2020**, *59*, 15741−15749; *Angew. Chem.* **2020**, *132*, 15871−15879.

[62] E. Baciocchi, M. F. Gerini, *J. Phys. Chem. A* **2004**, *108*, 2332−2338.

[63] C. J. O'Connor, *Prog. Inorg. Chem.* **1982**, *29*, 203–283.

[64] G. M. Sheldrick, *Acta Cryst. Sect. C.: Struct. Chem.* **2015**, *71*, 3–8.

[65] L. J. Barbour, *J. Supramol. Chem.* **2001**, *1*, 189–191.

[66] O. V. Dolomanov, L. J. Bourhis, R. J. Gildea, J. A. K. Howard, H. Puschmann, *J. Appl. Cryst.* **2009**. *42*, 339–341.